Dense shelf water production in the Adelie Depression, East Antarctica, 2004-2012: Impact of the Mertz Glacier calving

Maïté Lacarra, Marie-Noëlle Houssais, Christophe Herbaut, Emmanuelle Sultan, Mickael Beauverger

RESEARCH ARTICLE

Key Points:
- Variability of summer dense water properties in relation to winter convection
- Winter convection controlled by sea ice formation and deep stratification
- Lighter dense shelf water off Adélie Land after the Mertz calving

Correspondence to:
M. Lacarra,
maite.lacarra@locean-ipsl.upmc.fr

Dense shelf water production in the Adélie Depression, East Antarctica, 2004–2012: Impact of the Mertz Glacier calving

Maité Lacarra[1], Marie-Noëlle Houssais[1], Christophe Herbaut[1], Emmanuelle Sultan[1], and Mickael Beauverger[1,2]

[1]Sorbonne Universités (UPMC Univ, Paris 06)-CNRS-IRD-MNHN, LOCEAN Laboratory, Paris, France, [2]LM2E, Ifremer, Plouzané, France

Abstract Summer repeated hydrographic surveys and 4 years of mooring observations are used to characterize for the first time the interannual variability of the bottom water in the Mertz Glacier Polynya (MGP) on the East Antarctic shelf (142°E–146°E). Until 2010, large interannual variability was observed in the summer bottom salinity with year-to-year changes reaching 0.12 in Commonwealth Bay, the region with the highest sea ice production. The summer variability was shown to be linked to the efficiency of the convection during the preceding winter. The recent freshening of the bottom waters subsequent to the Mertz Glacier calving was well beyond the range of the precalving interannual variability. Within 2 years after the event, the bottom water of the shelf became too light to possibly contribute to renewal of the Antarctic Bottom Water. Rough estimates of the freshwater budget of the Adélie Depression indicate that the freshening necessary to compensate for net sea ice production in the MGP did not change drastically after the Mertz calving. The year-to-year salinity changes appeared to respond to the MGP activity. Yet, prior to the calving, the convective system in the polynya was also partly controlled by the late winter bottom salinity through a mechanism leading to a sequence of alternatively fresher and more saline bottom waters over the period 2007–2010. Exceptional events like the Mertz calving seem to be able to switch over the system into a less stratified state where convection responds more directly to changes in the surface forcing.

1. Introduction

Antarctic Bottom Water (AABW), the densest water mass of the world ocean, occupies the abyssal layer of the Southern Ocean as a relatively well-oxygenated, cold and fresh product, which spreads north into the Atlantic, Indian, and Pacific oceans. Surface water transformation on the continental margins around Antarctica and subsequent sinking of the dense shelf waters along the slope supply the bottom limb of the ocean thermohaline circulation. It has been argued that changes in the properties or formation rate of the AABW could affect the strength of the thermohaline circulation, and therefore the global climate [*Stouffer et al.*, 2007; *Purkey and Johnson*, 2012].

The production of AABW is considered to originate on the Antarctic shelf in coastal polynyas where near-freezing water (the so-called High-Salinity Shelf Water, HSSW) is formed through ocean surface cooling and brine drainage from growing sea ice. Upon mixing with ambient waters on the shelf and subsequent sinking and entrainment of Circumpolar Deep Water down the continental slope, these waters eventually acquire final AABW properties when reaching the abyssal layer of the Southern Ocean. While this process is suspected to occur at many locations around Antarctica, observations have unambiguously identified some primary formation sites: the Weddell Sea, the Ross Sea [*Carmack*, 1977], and the Adélie-George V Land [*Gordon and Tchernia*, 1972; *Rintoul*, 1998]. Estimates of the relative importance of these sites have evolved with time and are still subject to debate [*Jacobs*, 2004]. Additional sites like the Prydz Bay sector have been recently mentioned as potentially large contributors [*Orsi*, 2010; *Ohshima et al.*, 2013]. The Australian Antarctic Basin (AAB) collects bottom water from two of these sources, the Adélie Land Bottom Water (ALBW), considered as a local source formed on the shelf off the Adélie-George V Land and probably the larger contributor [*Rintoul*, 1998; *Orsi et al.*, 1999], and the Ross Sea Bottom Water (RSBW) which is advected from the Ross Sea to the east. The AAB has indeed the largest chlorofluorocarbon concentrations of the Southern Ocean [*Orsi et al.*, 1999], in agreement with the ALBW and the RSBW being the most important contributors

to AABW renewal. At the global scale, the AABW from the AAB has been recently recognized as responsible for changes observed in the abyssal layers of the North Pacific Ocean [*Masuda et al.*, 2010].

Several studies have reported significant changes in the properties of the AABW in the Australian Antarctic Basin during the past decades [*Whitworth*, 2002; *Aoki et al.*, 2005; *Rintoul*, 2007; *Johnson et al.*, 2008; *Shimada et al.*, 2012]. As often stated, such changes may just reflect changes in the properties or proportion of ambient water entrained or mixed with the source waters along their path across the basin. Recently, *Shimada et al.* [2012] proposed that increased vertical diffusion of heat into the RSBW layer during its transit to the AAB could explain the bottom warming in the AAB over the last two decades. Yet, when considering the bottom freshening of the AAB, there is also evidence that it may relate, at least partly, to freshening of the source dense waters from the Ross Sea and the Adélie/George V Land sector. According to *Rintoul* [2007], the bottom freshening observed across the AAB between 1995 and 2005 would require a freshwater input consistent with the mean freshwater input attributed to the floating ice loss in the Adélie Land sector over 1992–2002 by *Zwally et al.* [2005]. The likely influence of freshened dense shelf water from the Adélie Land sector is also consistent with the freshening of 0.03 identified over approximately the same period (1992–2004) in the AAB bottom layer at 140°E on the continental slope just downstream of the Adélie Land shelf [*Aoki et al.*, 2005]. Although *Shimada et al.* [2012] have recently suggested that a large (84%) part of the overall AAB freshening could be explained by observed changes in the transport and properties of the RSBW, they acknowledge that localized cooling (as opposed to basin wide warming) and enhanced freshening signals identified over the slope near the ALBW source region do indicate the influence of a fresher, colder, bottom water source there.

The source of the ALBW is found off the Adélie-George V Land, where HSSW, the precursor of the dense shelf water exported to the AAB, forms from brine rejection during sustained winter sea ice formation in the Mertz Glacier Polynya (MGP). The MGP is maintained by strong katabatic winds [*Wendler et al.*, 1997] and, until 2009, extended seaward in the lee of the Mertz Glacier Tongue (MGT) as a V-shape feature, forming one of the largest coastal polynyas of East Antarctica [*Massom et al.*, 1998]. The shape of the polynya drastically changed in February 2010 when the MGT broke and ice formerly blocked by the glacier was able to drift across the polynya region.

Changes in the dense shelf water properties, in particular salinity, on the continental margin are therefore expected to show a tight relationship to sea ice melt and/or growth. *Shadwick et al.* [2013] link the freshening of 0.15 of the dense shelf water observed in the Adélie Depression between 2008 and 2011 to reduced sea ice production in the reshaped MGP after the Mertz Glacier calving. Studying the impact of the glacier calving on ice production in the MGP, *Tamura et al.* [2012] indeed found that annual sea ice production in the polynya extending over the Adélie Depression and the Mertz Depression had reduced by 14% and 20% in 2010 and 2011, respectively, out of an annual mean of approximately 170 km^3 estimated over the pre-calving period (2000–2009).

Increased glacial melt can also lead to a fresher, less dense shelf product as the excess freshwater may be incorporated in the water column entrained into the dense water plumes during winter convection [*Galton-Fenzi et al.*, 2012]. Glacial melt may arise from enhanced contact of land or sea ice with relatively warm water, especially with the Modified Circumpolar Deep Water (MCDW) intruding on the shelf. Although there is no evidence that such a process did impact on the dense shelf water freshening observed in summer 2011 in the Adélie Depression, *Shadwick et al.* [2013] suggest that it may have contributed to the 1.16 m excess of freshwater added to the top 200 m of the Adélie Depression in that year, as a result of more ice being advected and melted into the region after the removal of the Mertz "barrier." With regards to dense water production, surface freshening increases the upper ocean vertical stability which in late summer-fall may alter preconditioning of the water column with regards to the following winter convection. This process was indeed shown to impact on the dense water production in the MGP in model simulations [*Marsland et al.*, 2004], but it could not be assessed from observations as this would require detailed knowledge of the spatial distribution and timing of the convection process which was missing.

Observations relevant to document the year-to-year variability in the Adélie Land region are very seldom. Off the shelf in the AAB, as well as on the Adélie Land shelf itself, most observational studies dealing with bottom freshening have concentrated on trends [*Whitworth*, 2002; *Aoki et al.*, 2005; *Rintoul*, 2007; *Shimada et al.*, 2012]. The repeat hydrographic stations were, however, too unevenly spaced in time to estimate year-

to-year changes and consequent aliasing on the estimated trends. In terms of dense water export from the shelf, adequate year-round monitoring of the Adélie Sill is still lacking, and evidence of substantial interannual variability in the export has so far only been provided by models [*Marsland et al.*, 2004; *Kusahara et al.*, 2011b]. Models, however, fail in reproducing accurately water mass property changes due to large biases. The present study aims at characterizing the interannual variability of the dense shelf water properties in the Adélie Depression over almost a decade (2004–2012) and to evaluate its possible link to sea ice melt or growth.

The period covered by our observations includes a particular event, the calving of a portion of the Mertz Glacier tongue in February 2010. Recurrent calving of the glacier is known to occur at time scales of several decades [e.g., *Frezzotti et al.*, 1998], yet the 2010 event appears as an "outstanding" perturbation to the "background" year-to-year variability in the context of the recent decade. *Kusahara et al.* [2011b] have estimated a substantial reduction of 23% of the dense export out of the Adélie Depression following the 2010 Mertz calving. This is about the same amount as the interannual variability (25–45% of the mean) found in a precalving simulation over the period 1979–2008 [*Kusahara et al.*, 2011b]. In the present study, we use observations to estimate the interannual variability of the dense shelf water prior to 2010 and evaluate the abrupt changes following the calving with regards to this variability.

Ideally, dense water properties should be monitored in winter. However, apart from the Mertz Glacier Polynya Experiment cruise on board, the RSV Aurora Australis in 1999 [*Bindoff et al.*, 2001; *Williams and Bindoff*, 2003] all hydrographic observations of sufficient spatial coverage in the Adélie Depression have been collected in spring and summer. Fortunately, a number of key geomorphic bottom features in the form of large depressions opened at shallow sills exist on the Adélie Land shelf which constitute natural permanent reservoirs for the winter dense products. Among these, the Adélie Depression between 142°E and 146°E, opened to the 420 m deep Adélie Sill, constitutes a major system collecting most of the dense product formed in the MGP [*Beaman et al.*, 2011]. Similar depressions, yet of smaller extent, exist in the coastal bays to the south of the Adélie Depression (Watt Bay and Commonwealth Bay). In order to characterize the interannual variability, we will use bottom water properties measured in these reservoirs in summer as the relevant indicator to infer the interannual variability of the dense water formation.

The summer data used here are hydrographic casts collected in the Adélie Depression during yearly cruises on board the French supply ship SV/Astrolabe from 2007 to 2012 in the context of the ALBION (Adélie Land Bottom water formation and Ice Ocean interactioNs) project [*Lacarra et al.*, 2011, hereafter L11]. These data are supplemented by CTD casts collected in 2004 and 2005 during the ICOTA (Ichtylogie COtière en Terre Adélie) cruises on board the same vessel [*Koubbi et al.*, 2011]. Additionally, in order to assess the link between winter and summer conditions, we document the annual cycle of water properties using a 4 year (2008–2011) time series of hydrographic properties collected at a mooring site in Commonwealth Bay, one of the small coastal depressions suspected to be the most efficient site with regards to the formation of HSSW (L11). To our knowledge, it is the first time that observations of a full annual cycle of ocean properties in the MGP are presented, and furthermore during four continuous years. These observations are further interpreted in relation to sea ice production in the polynya and to the regional-scale summer variability.

The paper is organized as follows. Section 2 is devoted to a description of the hydrographic observations and sea ice data. In section 3, results on the interannual variability of the dense shelf water summer properties are presented at some selected sites in the Adélie Depression. The results are interpreted in the context of the seasonal and interannual variability of water properties derived from mooring data and the sea ice production in the MGP. Section 4 is devoted to a discussion in which special attention is paid to the impact of the Mertz Calving. Our conclusions are presented in section 5.

2. Data

2.1. Ship Borne Hydrographic Observations

In order to document the interannual variability of the dense shelf water in the MGP, we use summer Conductivity-Temperature-Depth (CTD) data from successive cruises carried out every January from 2007 to 2012 (Figure 1). The hydrographic arrays sampled the various deeps of the polynya to the west of the MGT including the main Adélie Depression and the coastal bays. All casts extended from the surface down to the bottom. The 2008 CTD array provided the most extensive and complete survey of the area. Together with
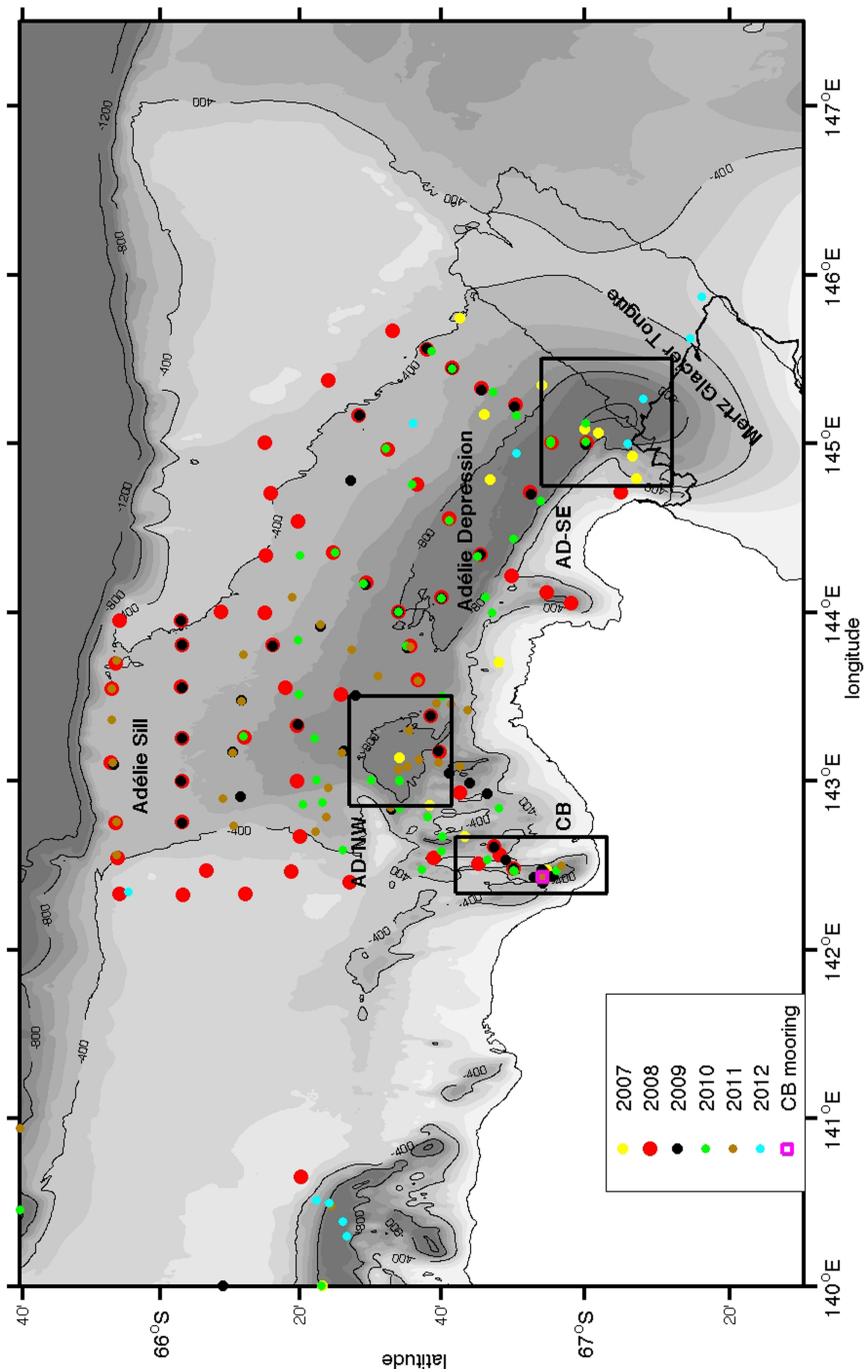
Figure 1. Distribution of the hydrographic casts collected during the six ALBION summer cruises (2007–2012) (see color codes for the different years on the map) on the ocean bathymetry [after *Beaman et al.*, 2011]. Also shown are the three regions where repeat CTD casts are used for the present analysis: Commonwealth Bay (CB), Adélie Depression Northwest (AD-NW), and Adélie Depression Southeast (AD-SE) and the mooring position in CB (magenta square). The Mertz Glacier Tongue (MGT) is also plotted with its precalving and postcalving geometry.

the CEAMARC-2008 observations and the ALBION-2009, it was used to characterize the summer water mass distribution in the depression (L11). While the original aim of the annual cruises was to document the interannual variability from repeat casts, highly variable and unpredictable ice and weather conditions hampered the systematic revisit of the same locations every year. However, three areas have been revisited almost every year over the period 2007–2012: Commonwealth Bay (CB), the northwest Adélie Depression

Table 1. Distribution of the Hydrographic Sensors Installed on the Commonwealth Bay Mooring Line Between January 2008 and January 2012: (M) SBE Microcats, (S) AADI Seaguard

Year	2008	2009	2010	2011
Location[a]	142°26′E–66°54′S	142°25′E–66°54′S	142°25′E–66°54′S	142°29′E–66°57′S
Period	13 Jan 2008–13 Jan 2009	14 Jan 2009–13 Jan 2010	13 Jan 2010–12 Jan 2011	18 Jan 2011–1 Mar 2012
Averaged	280 dbar (M)	220 dbar (M)	245 dbar (M)	306 dbar (M)
instrument levels	480 dbar (M)	420 dbar (M)	420 dbar (M)	596 dbar (M)
	700 dbar (M)	660 dbar (M)	610 dbar (S)	860 dbar (M)

[a]The year refers to the January month when the instrument recording started. In all years, the deepest instrument level corresponded to the bottom.

(AD-NW), and the southeast Adélie Depression (AD-SE; see black boxes in Figure 1). All three areas are considered as key areas with regards to dense water production (see next section). All selected CTD casts were collected within a few days time period every summer. Considering all years together, the envelope of the time period extends over 12–31 January in CB, over 14–19 January in AD-NW, and over 14–22 January in AD-SE.

In all years except 2010, the hydrographic profiles were obtained with a SeaBird Electronics SBE 9plus device supplemented for dissolved oxygen by a SBE43 sensor. In order to correct for possible sensor drift, all sensors have been calibrated in laboratory prior and after each cruise. Prior to 2011, water sampling could not be performed because the CTD winch on board the vessel could not support a rosette. In January 2008, however, the dissolved oxygen measurements could be corrected for a constant bias of 13.7 μmol L^{-1} through a comparison with the calibrated CEAMARC data at coinciding sites (see L11 for more details). Since 2011, a 12 bottle rosette frame has been added to the CTD device so that the conductivity and oxygen measurements could be calibrated based on water sample analyses. Dissolved oxygen was titrated using the Winkler method. Only in January 2010 were the CTD casts of the Adélie Depression carried out with a SBE25. However, following a failure of the system the same year, the SBE25 had to be replaced by a Microcat SBE37 for casts collected in CB. The SBE37 acquisition frequency was set at its maximum. SBE 9plus and SBE25 temperature and salinity measurements have nominal accuracy of ca. 0.001°C and 0.004, respectively. Note that despite all the difficulties encountered with the instrument sensors, we managed to construct a consistent set of hydrographic data having sufficient accuracy to make us confident in the results obtained from their analysis (see also L11 for more details about the data processing).

In order to complement the time series of hydrographic properties for earlier years, two CTD casts collected in 2004 and 2005 in AD-SE during ICOTA cruises have also been used.

2.2. Mooring Hydrographic Data

In order to relate the summer variability of the dense shelf water to the history of its winter formation, concomitant hydrographic data collected from moored instruments in Commonwealth Bay have been analyzed. A mooring line was maintained there at approximately the same location for 4 years (January 2008 to January 2012; Figure 1, magenta square; see also Table 1 for mooring location and description). It included up to three SBE 37 Microcats in the water column at roughly 250, 420, and 700 m (Table 1), the deepest level being always chosen near the bottom. The instruments recorded pressure, temperature, and conductivity at a 7.5 min sampling interval. In 2010, the bottom Microcat was replaced by an AADI Seaguard instrument which recorded pressure, temperature, and conductivity, all at a 10 min interval. The Seaguard was maintained near the bottom for 2 years and, in 2011, was moored together with a Microcat allowing some intercomparison between the two instruments. Microcat temperature and salinity measurements have nominal accuracy of less than 0.002°C and 0.001, respectively, with an accuracy roughly 1 order of magnitude lower for the corresponding Seaguard sensors. Regarding the Seaguard conductivity a large offset (on the order of 0.02 S m^{-1}) was discovered by comparison with the conductivity measured on a CTD cast at the mooring location in January 2010. A procedure was therefore implemented in order to correct the conductivities recorded by the Seaguard in 2010 (see Appendix A).

2.3. Sea Ice and Atmospheric Data

In order to relate the evolution of the dense water properties to surface air-sea ice interactions, estimates of the sea ice production and sea ice melt over the Adélie Depression have been made. The ice production

calculation is restricted to thin ice (i.e., ice with thickness less than 20 cm) as was proposed, for instance, by *Tamura et al.* [2008] when mapping sea ice production in Antarctic polynyas. The thin ice production is here assumed to represent the MGP production. Several algorithms to retrieve thin ice thickness from passive radiometer observations have been recently developed and evaluated [*Tamura et al.*, 2007; *Naoki et al.*, 2008; *Kaleschke et al.*, 2012]. In the present study, the thin ice thickness was estimated following a methodology adapted from the *Tamura et al.* [2007] algorithm. The latter is based on a piece-wise linear relationship between the thin ice thickness and the polarization ratios, PR_{37} and PR_{85}, derived from the SSM/I brightness temperatures. We adapted the algorithm so that thin ice thickness could be retrieved at a 6.25 km resolution from the Aqua AMSR-E 36 GHz and 89 GHz vertically and horizontally polarized brightness temperatures. Following a methodology suggested by *Martin et al.* [2005], we used daily linear regressions of the AMSR-E PR_{36} and PR_{89} onto the SSM/I PR_{37} and PR_{85}, respectively, in order to inject PR_{36} and PR_{89} values into the *Tamura et al.* [2007] algorithm. The linear regressions were performed at the resolution of the SSM/I observations, that is, 12.5 and 25 km for the PR_{37} and PR_{85} regressions, respectively. The AMSR-E brightness temperatures were obtained from NSIDC over the period 2002–2011 [*Cavalieri et al.*, 2004] and sea ice concentrations (SIC) derived at the same resolution through the ASI algorithm [*Spreen et al.*, 2008] were obtained from the University of Hamburg (ftp://ftp-projects.zmaw.de/seaice/AMSR-E_ASI_IceConc/tmp_no_landmask/hdf/s6250/). Sea ice production over thin ice was then calculated using surface atmospheric forcing fields from the ERA-I reanalysis [*Dee et al.*, 2011] over the same period. Following *Parkinson and Washington* [1979] the total surface atmospheric heat flux was obtained from an estimate of the ice surface temperature assuming a balance between the atmospheric flux and the conductive heat flux through the ice. In this balance, the outgoing longwave radiation and the turbulent heat fluxes were linearized around the ice surface temperature, the turbulent fluxes being estimated from bulk formulae in which the heat transfer coefficient was chosen to be 1.3×10^{-3} [*Inoue et al.*, 2003]. Fast ice is discriminated from thin ice using a criteria based on the 20 day averaged vertically polarized brightness temperature, TV_{89} (see, e.g., the discussion in *Tamura et al.* [2007]). The time scale of 20 days was suggested by *Fraser et al.* [2010] as a relevant time scale to map the East Antarctic fast ice variability. Polynya grid cells with TV_{89} lower than a threshold value were eliminated. The threshold value was determined based on a comparison of the TV_{89} probability density functions between years assumed to be characterized by little fast ice in our region of interest (i.e., prior to 2010, see *Fraser et al.* [2012] climatology for the period 2000–2008) and years expected to show fast ice or icebergs (i.e., starting in 2010, after the Mertz calving).

In this study, we present time series of the cumulated ice production over the freezing days of a full year, freezing days being defined as those for which the ice surface sustains a heat loss to the atmosphere. Note that, for the period October-November-December 2011, AMSR-E data were lacking after the sensor stopped operating. Ice production for that period was estimated using thin ice thickness derived from the SSM/I sensor following the *Tamura et al.* [2007] algorithm.

In parallel, estimates of the sea ice melt due to the atmospheric heat flux have been obtained based on the SSM/I 12.5 km resolution SIC derived through the ASI algorithm at Ifremer/CERSAT (ftp://ftp.ifremer.fr/ifremer/cersat/products/gridded/psi-concentration/data/antarctic/daily/netcdf/). As for the ice production, the melt rates were calculated using the ERA-I forcing fields and cumulated over the melt days defined as those for which the surface heat budget of the ice surface indicates a heat gain for a prescribed ice thickness. Different ice thicknesses have been tested in order to estimate a possible range of melt rates. The melt rates are presented here for a prescribed summer ice thickness of 3 m considered as a reasonable average for the drift ice in the region but actually applied to all ice types including thick land and fast ice.

Both production and melt were averaged over a region of approximately 31,000 km^2 (AD-tot) encompassing the entire Adélie Depression and chosen to include most of those MGP new ice production regions where the brine-induced dense water is expected to drain into the deep reservoir of the depression (Figure 1). Separate estimates were also performed for CB.

3. Results

3.1. Mean Characteristics of the Water Mass Distribution Over 2004–2012

We focus on the Adélie Depression region which is expected to collect most of the HSSW formed in winter in the MGP. The depression is actually made of an ensemble of individual basins. The depression itself,
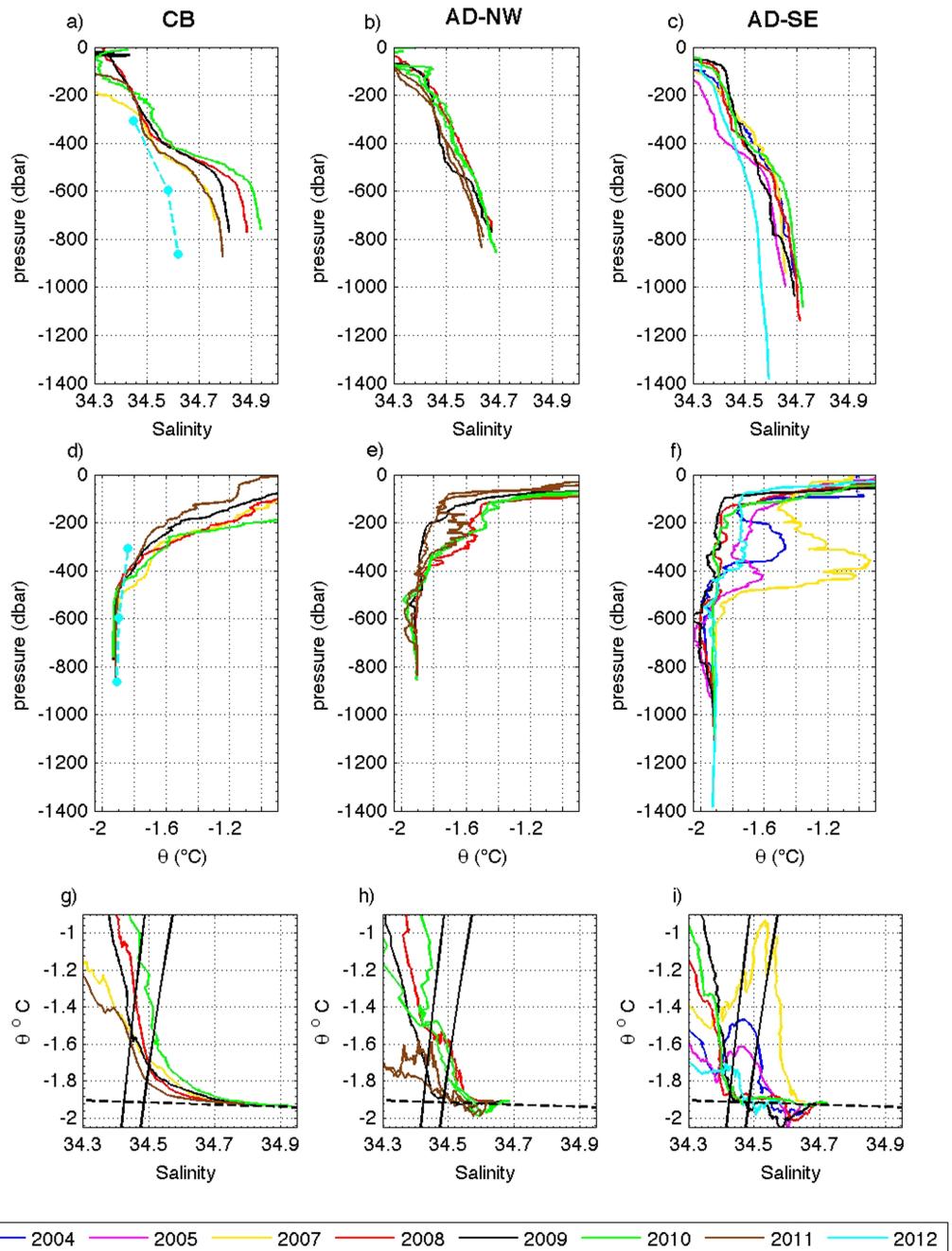
Figure 2. Vertical distribution of (a–c) salinity and (d–f) potential temperature (in °C) as well as (g–i) θ-S diagrams, obtained from CTD casts performed in January in the three regions of the study: (left) CB, (middle) AD-NW, and (right) AD-SE. Different colors refer to the different years of the period 2004–2012. In Figures 2a and 2d, the 2012 salinity and temperature are obtained from the data recorded on 20 January 2012 by the Microcats deployed at three different levels (302, 589, and 850 m) on the mooring line. In Figures 2g–2i, the two black curves indicate the $\gamma^n = 28.00$ and $\gamma^n = 28.27$ kg m^{-3} neutral density surfaces and the dashed black line represents the freezing point of seawater at 30 dbar.

made of two subbasins separated by a deep ridge, is the largest reservoir in the area and is connected to the deep ocean through the Adélie Sill and to the small basins enclosed in the southern coastal bays (Commonwealth Bay and Watt Bay) through shallow sills (ca. 400 m) (*Beaman et al.* [2011] and L11 for a detailed description of the local bathymetry). Such a configuration allows bottom waters with distinct summer salinities to be stored in the different basins as a result of limited inter basin exchanges. In order to study the year-to-year variability of these waters, we therefore selected three different sites, each of them

representative of a different basin (Figure 1). The three sites were also selected because they have been monitored through repeat hydrographic casts almost every year during the considered period (2004–2012). Two sites are in the Adélie Depression, one being in the shallowest northwest subbasin (AD-NW, maximum depth of ca. 860 m) and the other in the deepest main subbasin (AD-SE, maximum depth of ca. 1300 m). A third site has been chosen in Commonwealth Bay where the depression there reaches ca. 870 m.

All three sites showed signature of a cold, saline (Figure 2), and high oxygen content (not shown) water mass at the bottom, which was identified as dense shelf water according to the minimum neutral density criteria of 28.27 defined by *Whitworth et al.* [1998]. Earlier summer cruises [e.g., *Vaillancourt et al.*, 2003] have already revealed the presence of HSSW as a dense ($\sigma > 27.88$, following *Bindoff et al.* [2000] criteria) product in the depression (L11). Analyzing in more details the summer 2008 observations, L11 noticed spatial contrasts in its properties with the highest bottom salinity encountered in CB, where it was higher by as much as 0.35 (0.13) than in Watt Bay (Adélie Depression), respectively. The contrast is confirmed in all years presented here. Consistently, the 2008–2010 averaged bottom salinity in CB is 34.88 while it is only 34.70 in AD-SE and is even fresher (34.67) in AD-NW. In agreement with L11 findings in 2008, no MCDW (a warm water mass at intermediate depths) or Ice Shelf Water (ISW, a comparatively fresh and cold water mass with temperature lower than the freezing point at near-surface pressure) are found in CB in summer in any of the sampled years while both water masses are present in the Adélie Depression (Figures 2g–2i). The signatures of the MCDW and ISW are, however, stronger in AD-SE than in AD-NW with the former region hosting a colder mode of ISW due to its proximity to the Mertz Glacier, and a warmer and saltier mode of MCDW. The MCDW distribution is again in agreement with L11 who suggested that in 2008 the MCDW penetrated on the shelf from the eastern Adélie Sill along the western edge of the MGT.

3.2. Interannual Variability of Hydrographic Properties

Figures 2a–2f show the salinity and temperature profiles collected at the three sites: CB, AD-NW, and AD-SE for different summers over 2004–2012. Note that, at all three sites, data are lacking in 2006 and that there were no data in AD-NW prior to 2008 and in CB prior to 2007. Moreover, as a consequence of the Mertz calving in February 2010, the AD-SE site was unreachable in summer 2011. The giant iceberg (B-9B), originally grounded to the east of the glacier tongue, migrated westward after the calving into the Adélie Depression to occupy a more or less stationary position over the AD-SE site throughout the summer 2011. For the same reason, in 2012, site AD-NW and site CB were unreachable after berg B-9B continued its westward drift during the fall 2011 and regrounded to the north of CB. Some information about the 2012 hydrography in CB was, however, obtained from the data collected by the three Microcats on the mooring (cyan dots in Figures 2a and 2d).

Significant interannual variability can be seen in the salinity profiles at all three sites. In CB, salinity shows a vertical structure representative of a two-layer system with the main halocline (or equivalently pycnocline) lying in the 400–480 m range, roughly corresponding to the sill depth (Figure 2a). On average over 2007–2011, the density difference across that level is $\Delta \rho = 0.22 \pm 0.06$ kg m^{-3}. The same structure is also observed for temperature with a main thermocline overlying a fairly homogeneous deep layer at freezing temperature (Figure 2d). The interannual variability in salinity is larger in the deep layer than above the halocline, with a salinity standard deviation (std) at 700 dbar of 0.125 over 2007–2012 (the 2012 value has been linearly interpolated between salinity recorded by the Microcats at 600 and 870 dbar) which is almost five times higher than the std at 300 dbar. Consistently, the density increase across the main halocline is strongly correlated (0.97, $p = 0.005$) with the bottom density (or, alternatively, salinity) while the correlation is insignificant with the density at 300 dbar. The deep temperatures, on the other hand, are constrained by surface freezing and show little interannual variability (the rms difference between the freezing point and the potential temperature at the bottom, both referred to 30 dbar is ca. $10^{-2\circ}$C).

In the Adélie Depression, the two-layer structure is not as easily identified in CB although on average the salinity gradient at most stations is enhanced in the 350–500 m range (again at the level of the Adélie Sill) with a density step $\Delta \rho = 0.13 \pm 0.03$ kg m^{-3} smaller than in CB (Figures 2b and 2c). The range of interannual variability for salinity is less contrasted in the vertical, still with higher amplitude changes in the deep layer (std on the order of 0.05). There are signs of strong exchanges with the surroundings at all levels. Below 500 m, signatures of ISW are seen in 2010 and 2011 in AD-NW and almost every year except in 2007 in AD-SE (Figures 2e and 2f). The large year-to-year temperature changes at these levels are likely
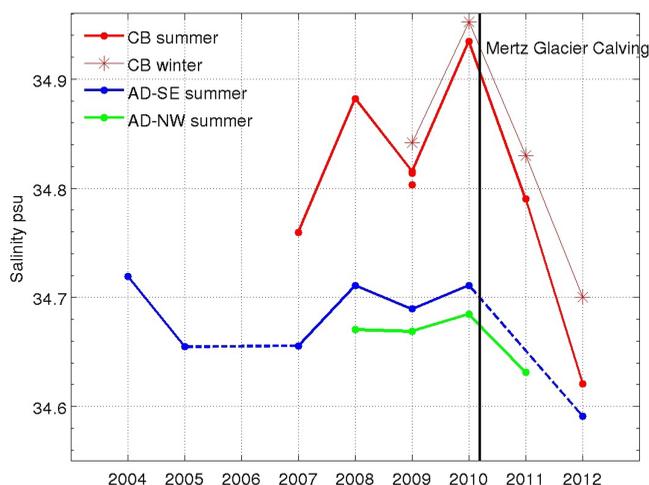
Figure 3. Time series of the summer bottom salinity in CB (red dots), AD-NW (green dots), and AD-SE (blue dots) as measured during the CTD cruises in 2004–2012. Also shown as red stars is the bottom salinity measured at the CB mooring at the end of the convective period during the preceding winter.

dominated by the effect of such transient (in time and space) ISW intrusions rather than a sign of interannual variability. The intrusions, however, do not reach to the bottom and a bottom layer with fairly constant temperature is preserved on all profiles.

Time series of the bottom salinities in summer are shown in Figure 3. Prior to the Mertz calving, the interannual variability of the salinity is large at all three sites and is again the highest in CB, with year-to-year changes reaching 0.12 and a std of 0.077 over 2007–2010, while the std reduces to only 0.026 in AD-SE. At all three sites the spatial variations of the bottom salinity across the surrounding subbasin are in the range 0.003–0.009 (depending on the site and the year) so that the interannual variability is in all cases larger. Therefore, the observed time changes are not artifacts due to the different sampling locations from one year to another. Note however that the CTD cast in 2007 in CB was performed higher up (by some 100 m) on the depression slope, which may explain the particularly low salinity value recorded in CB in that year (a weak vertical salinity gradient always persists in the deep layer in summer). Despite different amplitude, the variability of the bottom salinity is in phase between the three sites.

At all three sites, the bottom water properties changed significantly following the Mertz calving with a steady decrease of the salinity in the two consecutive 2011 and 2012 summers (Figure 3). There was a large drop in bottom salinity between 2010 and 2011 (0.15 at CB and 0.05 at AD-NW), and again between 2011 and 2012 (0.17 at CB), which converts into a cumulated decrease of 0.12 at AD-SE between 2010 and 2012. The large drop in bottom salinity translates into a large increase of the freshwater content of the Adélie Depression (AD-SE) and the CB depression (Figures 4a and 4b, blue lines). At all sites the decrease per year over this period is twice as much as the std over the precalving period. The decrease in bottom salinity is associated with a weaker stratification at intermediate depths (Figures 2a–2c), $\Delta\rho$ reaching at all sites in 2012 an absolute minimum for the entire period. The time series of $\Delta\rho/\rho$ at CB (AD-SE), shown as a red dashed line in Figures 4a and 4b, indeed show that the 2011 (2012) values fall beyond almost two std of the corresponding 2007–2010 time series (the std in CB and AD-SE are 4.8×10^{-5} and 2.4×10^{-5}, respectively). The decrease in salinity also goes with a decrease in the bottom oxygen content. In CB, the latter decreased from 343 μmol L^{-1} in 2008 to 324 μmol L^{-1} in 2011 while in AD-SE, the oxygen decreases from 323 μmol L^{-1} in 2008 to 317 μmol L^{-1} in 2012. The latter difference is larger than possible differences arising from spatial heterogeneity which, in 2008, were characterized by a std of no more than 2 μmol L^{-1}.
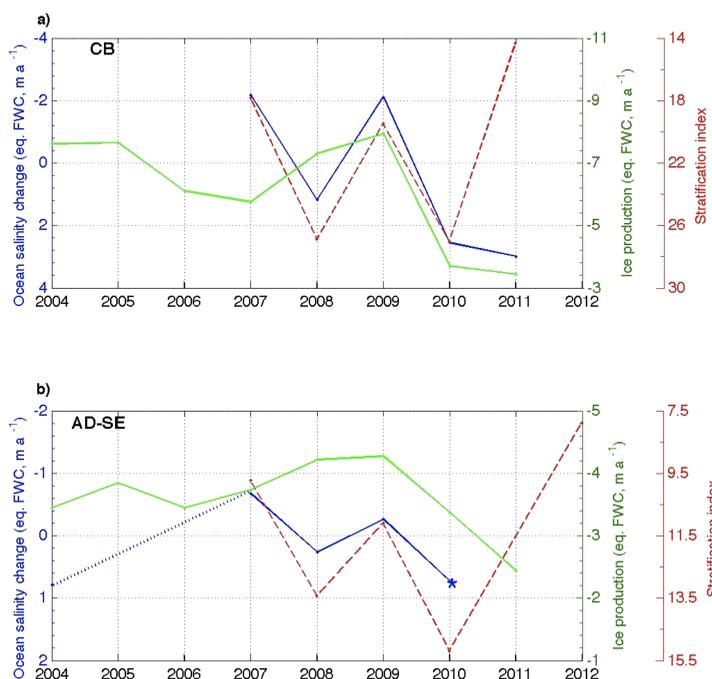
3.3. Winter Versus Summer Properties: Seasonal Monitoring in Commonwealth Bay

The mooring deployed from January 2008 to March 2012 in CB allowed us to analyze the relationship between the dense shelf water properties observed in summer and those observed in winter. The three Microcats continuously recorded four annual cycles of the pressure, temperature, and conductivity at roughly 250 dbar, 450 dbar (600 dbar in 2011) and at the bottom (Table 1 and Figure 5). While in the first 3 years, the mooring was maintained at roughly the same position on the northern slope of the bay depression, in 2011, it was moved some 7 km southward and occupied the deepest part of the depression.

Prior to the Mertz calving, a strong seasonal cycle links the winter and summer properties at all levels and in all years (Figure 5). Gradual destratification of the water column below ca. 250 m starts in early to mid-March depending on the year. In a salinity-stratified water column, convective mixing is first identified by a

Figure 4. Bottom salinity change between January of the abscissa year and the following January (blue line, left axis), annual sea ice production (green line, first right axis), both converted to equivalent freshwater changes (in m a^{-1}), and summer stratification index based on the relative density change ($10^5\ \Delta\rho/\rho$) across the main halocline (dashed red line, second right axis) in CB over the period 2004–2011. (b) Same as Figure 4a except in AD-SE (and AD-tot for the ice production). In Figures 4a and 4b, salinity changes and ice production have been converted to equivalent freshwater changes using a reference ocean salinity of 34.50 and, for the salinity change, a mean water depth of 610 m in CB and 420 m in AD. Note that all vertical axes show increasing values downward and that the axis ranges are twice as large in CB as in AD-SE. The CB and AD-tot domains used to calculate the averaged sea ice production are shown as black boxes in Figure 6, CB (AD-tot) being the smaller (larger) domain. In Figure 4b, the star symbol in 2010 represents an estimate of the annual freshwater content change in AD-SE based on the difference between January 2010 and January 2012. Consistently, the sea ice production in 2010 in AD-tot is an average of the production over 2010–2011. The 2012 value of the stratification index in AD-SE is shown to highlight the tendency to a reduced stratification in the Adélie Depression after 2010.

decrease in salinity and temperature which traces entrainment of the fresh, cold upper layer into the saltier, warmer lower layer (Figures 5a and 5b). The salinity subsequently increases as brines rejected from the newly formed ice contribute to salinize the convective layer. Prior to the Mertz calving, this process gradually reached to the bottom where the salinity started to increase from early to late June to reach a maximum at the end of the winter (September-October). At the same time, the bottom temperature was lowered to the freezing point and remained close to this temperature throughout the convective period (Figure 5c). The amplitude of the seasonal bottom salinity change across the convective period is 0.077 in 2008 and 0.240 in 2009, in the range of the interannual variability. The salinity increase due to convection is counteracted at all levels by a regular background freshening which is the most visible outside the convective period, in particular during the spring restratification period. The freshening is associated with some warming at all levels (Figures 5b and 5c). After the Mertz calving, convective mixing slows down so that in 2010, signatures of homogenization (better identified on the raw time series, not shown) are still seen at 400 m depth but do not reach the bottom layer, while in 2011 only a few events of mixing down to 600 m are detected in "April-May" and later in August. Without being supplied by salty convective plumes, the bottom layer undergoes a gradual freshening over 2010–2011. Overall, the year-to-year variations of the summer (January) salinity are very similar to the variations of the maximum salinity reached at the end of the previous convective period (compare red dots and stars in Figure 3), suggesting that the deep bay reservoir has a several months memory with regards to bottom water properties and that these properties are less affected by interannual variations in the background freshening than by the convection.

The evolution of the bottom salinity is likely linked to the ability of the convection to bring salt into the bottom layer. In particular, the important decrease in the bottom salinity of the depression observed in the postcalving years would reflect the absence of renewal of this layer as a result of weak convective activity.
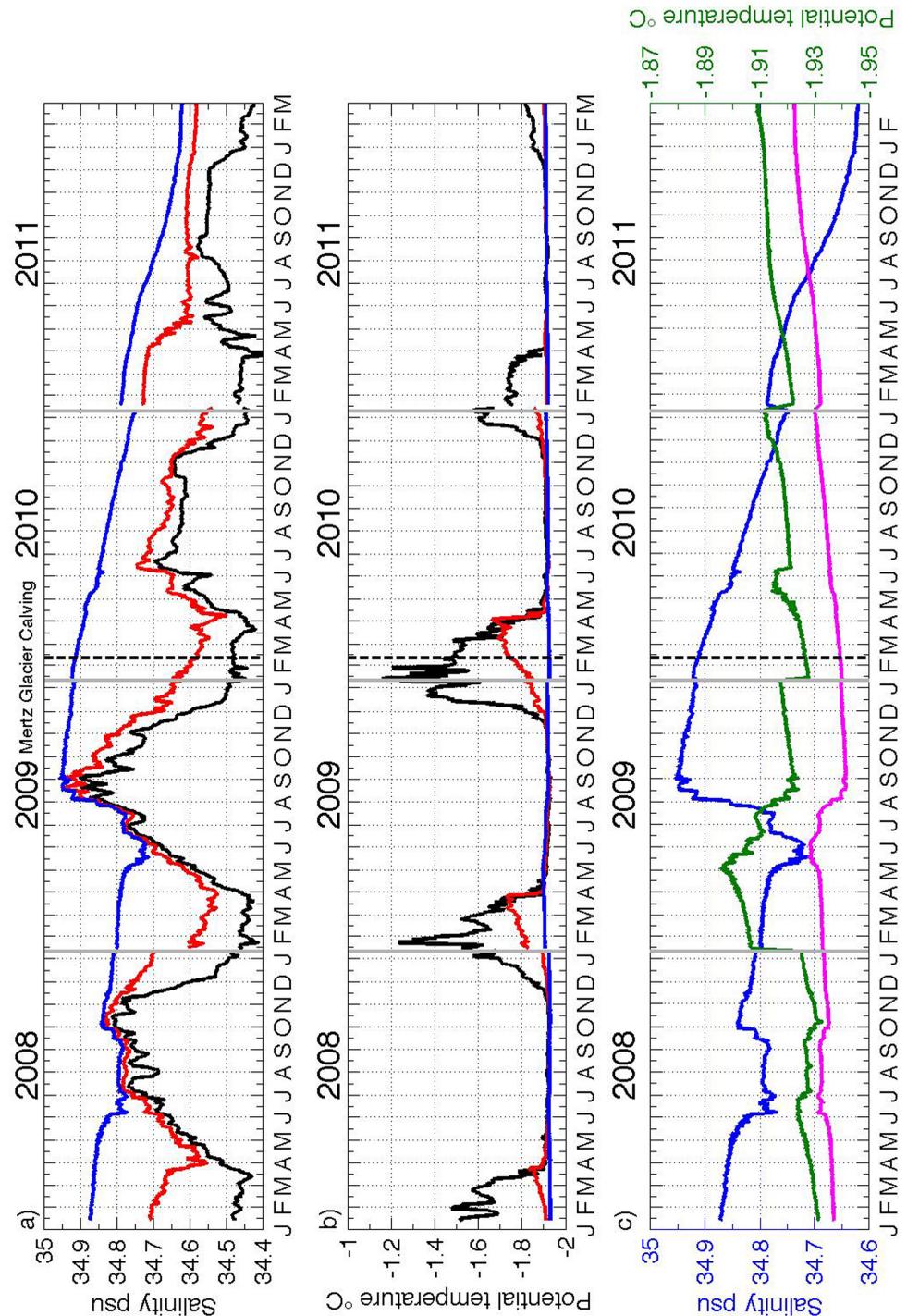
Figure 5. Time series of (a) salinity and (b) temperature (in °C) recorded by the top (black), intermediate (red), and bottom (blue) instruments on the CB mooring between January 2008 and January 2012 (see Table 1 for details on the instrument depths and recording periods). (c) Time series of the bottom potential temperature referred to 30 dbar (green curve, right axis) and salinity (blue curve, left axis) together with the freezing point at 30 dbar (magenta curve). Note the enhanced temperature scale compared to Figure 5b. In Figures 5a–5c, the vertical dashed line in February 2010 marks the date of the Mertz calving. All data were acquired using SBE Microcats except in 2010 when an AADI Seaguard was used at the bottom level instead of a Microcat.

The duration of the homogeneous period at CB in both 2008 and 2009 is fairly similar (roughly 3 months) but the timing of the period differs, year 2009 showing earlier start of the homogenization (June) compared with 2008 (July). While both years show episodes of restratification lasting several days during the
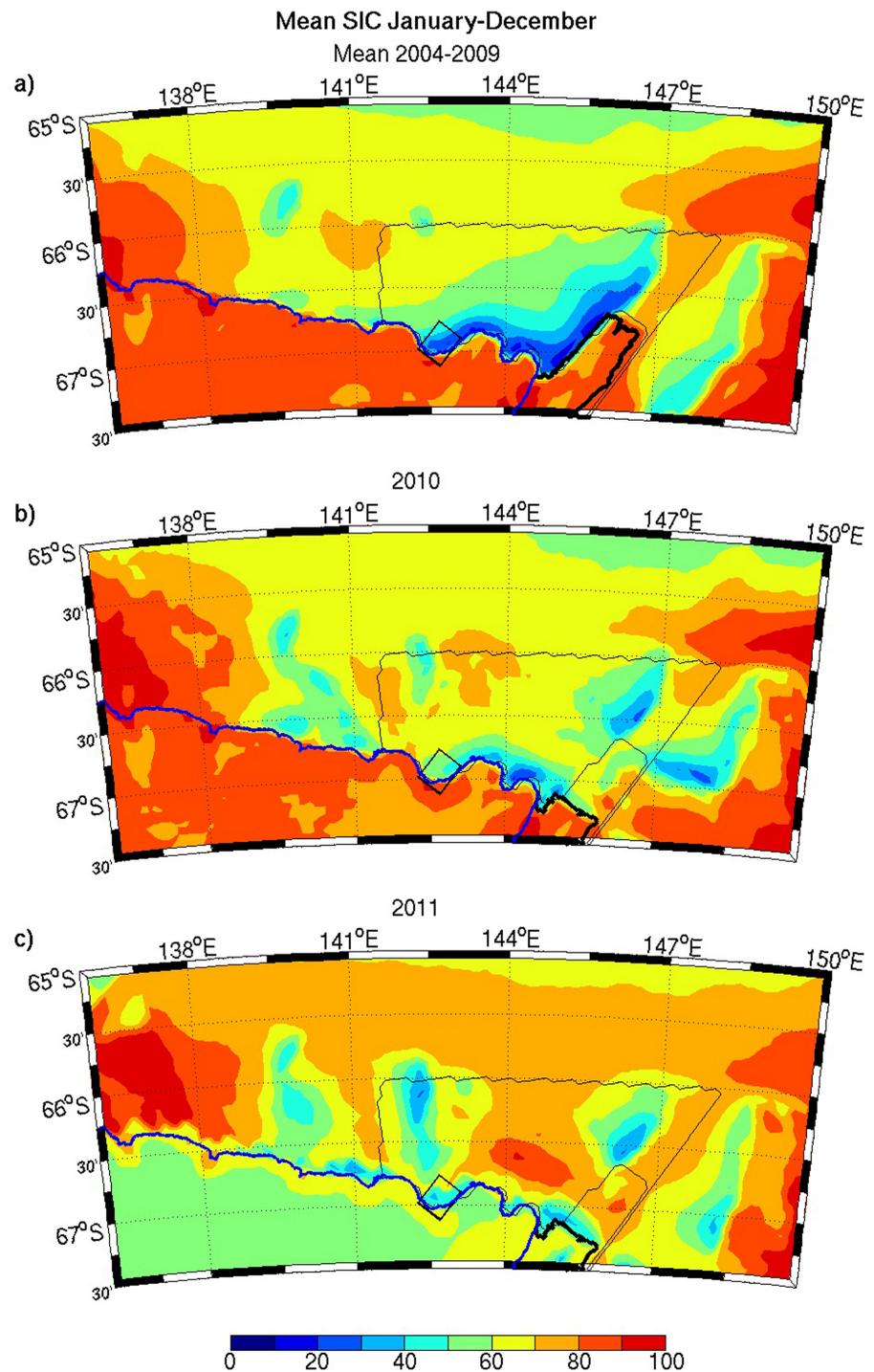
Figure 6. Mean annual sea ice concentration (in %) in (a) 2004–2009, (b) 2010, and (c) 2011. The 2004–2009 distribution is an average over the 6 years and characterizes the precalving situation. Also shown as black boxes are the two regions, AD-tot and CB, used to estimate the ice production. The contour of the Mertz Glacier Tongue is plotted with its (a) precalving and (b and c) postcalving geometry.

homogeneous period, these episodes are stronger and more frequent in 2008 and certainly limit the salinization of the bottom layer during that period.

3.4. Interannual Variability of Sea Ice Production and Melt
As shown above, the time evolution of the bottom salinity in CB is likely to be related to the haline convection activity in the previous winter. A similar relationship should also prevail in the Adélie Depression itself

although it is certainly more complicated due to the likely impact of advection by ocean currents and mixing with different ambient water masses. In order to understand the variability of the haline convection in both regions, time series of the sea ice production have been calculated over the AMSR-E period, both for the entire Adélie Depression on a domain extending between 141°30′E and 148°E and between 66°S and 67°20′S (AD-tot) and for CB (see domains shown as black boxes in Figure 6). Note that the CB domain is restricted to the inner bay which has mostly remained out of reach of iceberg B-9B in 2011 and 2012. The precalving (2004–2009) annual sea ice production is 190 km^3 a^{-1} in AD-tot with a std of 18 km^3 a^{-1} and the highest production rates found in CB. Assuming a sea ice salinity of 10 and a reference ocean salinity of 34.50, these values convert into a freshwater removal of 3.9 m from the water column, on average over the domain. In 2008 and 2009, the cumulated productions are very similar (Figure 4, green lines) and, together with 2003 (not shown), are among the most highly productive years.

Both in the entire region and in CB, the cumulated production is drastically reduced in 2010. Compared with the precalving mean, the reduction is larger in CB (48%) than in AD-tot (12%) and, in the latter region, is mainly due to a reduction of the polynya extent. In 2011, ice production remains at the 2010 level in CB while in AD-tot it is again reduced, and to a larger extent (24% of the precalving mean) as a result of both reduced polynya extent and weaker air-sea heat fluxes over the polynya. The reduction of the polynya extent after the Mertz calving is clearly visible on the SIC distributions shown in Figure 6 where the area of ice with SIC < 60% is indeed greatly reduced in 2010 and 2011 compared with the precalving mean.

Structural changes in the MGP distribution which are consistent with the previously mentioned reduction of the winter polynya extent occurred subsequent to the Mertz calving [e.g., *Tamura et al.*, 2012]. The breaking of the glacier tongue indeed removed what constituted an efficient barrier to the westward advection of ice into the Adélie Depression. Increasing import of ice into the region has certainly contributed to the decrease of the MGP activity after the Mertz calving. Concomitantly, a more compact sea ice cover in the warm season could significantly increase the amount of sea ice melt within the depression, thus altering the regional freshwater budget. Estimates of the atmospheric sea ice melt for the AD-tot domain were therefore produced according to the procedure described in section 2. While on average the annual sea ice melt in the precalving period (4.5 km^3 a^{-1}) is negligible compared with the sea ice production, its variability is comparatively large (2.2 km^3 a^{-1}). Moreover, it increases substantially after the calving, most abruptly in 2011, the annual increase (compared to the 2004–2009 precalving period) over 2010–2011 reaching twice the precalving std. The excess freshwater input of 0.11 m a^{-1} to the water column over 2010–2011 represents more than 10% of the concomitant deficit due to reduced sea ice production (0.92 m a^{-1}).

4. Discussion

Hydrographic observations carried out in the MGP on summer cruises on board the S/V Astrolabe over the period 2004–2012 have been used here to document for the first time the year-to-year variability of the dense shelf water properties. The period includes an outstanding event, the calving of a large part of the Mertz Glacier tongue in February 2010, which has led to abrupt changes in the ice environment. Our observations are unique in the sense that they allow us to estimate the interannual variability prior to the calving, to characterize the precalving situation of January 2010, and to evaluate the modifications of the dense shelf water properties with regards to the precalving situation during the following years.

Prior to the calving, we already observed large year-to-year variations of the bottom water properties in the Adélie Depression which were in phase across the different sampled sites. In the deepest part of the Adélie Depression (AD-SE), salinity variations could exceed 0.06 but were smaller closer to the sill (AD-NW), which was interpreted as a sign of mixing of the dense water with the ambient shelf waters as it proceeds toward the sill. The particular environment of Commonwealth Bay, with its individual basin geometry and its highest annual sea ice production, offers favorable conditions for observing the strongest impact of brine-induced haline convection on the dense water mass. Between 5 and 8 m of freshwater were removed from the water column every year through ice formation (Figure 4a, green line), which was about twice as much as in the Adélie Depression (Figure 4b, green line). As a consequence, year-to-year bottom salinity variations there were on average three times as high as in the Adélie Depression.

The Mertz calving brought out large oceanic changes across the MGP. An overall freshening of the water column was observed everywhere from 500 m to the bottom over 2010–2012. The vertical distribution of

this freshening from the few available stations in summer appears fairly uniform below 600 m (Figure 2). Assuming that the observed decrease in bottom salinity can be used for a rough estimate of the freshwater content change in this depth range, an excess of 1.40 m of freshwater would have been added to the deep layer in AD-SE, and even more (1.80 m) in CB, between January 2010 and January 2012.

The bottom waters of the Adélie Depression become significantly lighter in 2011 and 2012, which questions their ability to form AABW. According to the summer clockwise circulation scheme suggested by *Kusahara et al*. [2011b] for the Adélie Depression, the western depression (AD-NW) should collect the dense shelf water flowing from the southeastern depression toward the Adélie Sill. In 2011, bottom water with salinity 34.63 was observed in AD-NW which, according to the minimum density criteria of $\sigma_0 = 27.88$ proposed by *Bindoff et al*. [2000] would be dense enough to form AABW. In 2012, we do not have observations in that region. However, if a density correction derived from the mean difference between AD-SE and AD-NW bottom values over 2008–2010 is applied to the bottom density recorded in AD-SE in 2012, the bottom waters in AD-NW in 2012 would have density not exceeding $\sigma_0 = 27.83$ implying that the summer overflow could not supply the AABW layer of the AAB.

Several processes can explain the freshening of the dense shelf water after the Mertz calving. Earlier studies have already pointed to the decrease of the sea ice production in the MGP after the calving [*Tamura et al*., 2012, *Kusahara et al*., 2011b]. Freshening and reduced export of the dense shelf water formed in the Mertz region under a changing climate was also associated with reduced polynya activity [*Marsland et al*., 2007]. Our results confirm this finding when considering the total depression with a cumulative decrease of almost 90 km³ of ice production over the, 2010–2011, 2 year period (or equivalently 45 km³ a⁻¹) compared to the 2004–2009 precalving period while at the same time the bottom salinity drops by 0.12. Both changes amount to three to four times the respective precalving standard deviation. That the polynya activity controls the bottom water properties is confirmed and better assessed in CB where two consecutive years of observations are available following the calving. After the Mertz calving, between the summer 2010 and the summer 2012, the bottom salinity in CB decreased at a fairly steady rate (Figure 3) roughly corresponding to an increase of 3 m a⁻¹ of the freshwater content of the bay reservoir in both 2010 and 2011 (Figure 4a, blue line). This steady salinity decrease is consistent with the persistently reduced winter ice production starting in 2010 after the production rate dropped to a level of roughly 50% of the winter 2009 value (Figure 4a, green line). In contrast, the additional freshwater sources necessary to close the freshwater budget of the reservoir (obtained from the difference between the freshening of the reservoir and the contribution of the ice production) remained almost stable after 2010 and therefore do not seem to have contributed to accelerating the freshening of the reservoir after the calving. Mooring observations at CB in 2010 and 2011 suggest that the bottom freshening is linked to lack of renewal of the bottom layer during these years. In 2011, this happens despite the tendency of the deep water column to become less stratified (Figure 4a, red dashed line).

While the above results would suggest a potential for the year-to-year evolution of the dense water properties to be inferred from sea ice production, we notice that, prior to the Mertz calving, there is no tight relationship between annual sea ice production and the annual salinity change in either region (Figures 4a and 4b). In both sites, for instance, year 2007 is characterized by a substantial salinity increase while the ice production is relatively low. On the contrary, year 2008 is characterized by a substantial salinity decrease while the ice production is relatively high. On the other hand during this precalving period, the annual bottom salinity change closely follows the evolution of the deep stratification during the summer preceding the convective period, as measured by the density step across the main halocline (Figures 4a and 4b, blue and red lines). The apparent 2 year cycle in the stratification and salinity change over 2007–2010 suggests an internal feedback between the bottom salinity and the convection in which the saltier the bottom water at the end of the winter, the stronger the main pycnocline and the deep stratification in the following summer-fall and the weaker the convection the next winter leading to lower bottom salinity, and so on. This feedback is only made possible by the existence of topographic reservoirs which limit the impact of exchanges with the surroundings on the bottom water properties. It should be noted that, by convection efficiency, we mean the capacity of the convection to counteract the tendency of the system to restratify (e.g., by lateral mixing through baroclinic instability).

Signatures of active restratification are obvious in the salinity and temperature records at the upper two Microcats of the mooring in CB in 2008–2009 (Figure 5). Restratification occurs through freshening/warming events which are clearly identified in the upper layer during the convective period, or more continuously as a steep freshening/warming trend during the so-called restratification phase following the homogenous phase. While in both years convection reached down to the bottom, stronger (weaker) January stratification in 2008 (2009) led to more (less) efficient restratification of the upper water column, precluding (enhancing) salt accumulation in the bottom layer during the convective period. More efficient restratification may occur through incorporation of more stratified water from the surroundings or through a more baroclinically unstable convective patch as a result of sharper horizontal gradients. Strong deep stratification in summer 2010 as a result of efficient haline convection in winter 2009 may also have contributed to reduce the convection activity in winter 2010, but, in this case, the effect cannot be isolated from that of the reduced ice production. The stratification evolution throughout the region (Figures 4a and 4b), most notably its sustained decrease in 2011 and 2012, also suggests that as a consequence of the Mertz calving, the convective system in the MGP has switched over to a new state, i.e., from a stratification-controlled state to a surface forcing-controlled state. This would be because lack of bottom water renewal after the calving has definitely destratified the water column, which would be now more sensitive to the surface forcing. Recent studies [*Shadwick et al.*, 2013] have highlighted a concomitant large mixed layer freshening in the Adélie Depression subsequent to the Mertz calving, which would lead to an increasingly stratified upper ocean. Our conclusions highlight the equal importance of the deep stratification with regards to the evolution of bottom water properties.

Since February 2010, the shorter Mertz Glacier Tongue has reduced the barrier effect for the sea ice drifting from the east into the depression leading to increased sea ice coverage throughout the year. A simple calculation of the area of the melting ice indicates an abrupt increase in 2011 (not shown). Although this increase to some extent reflects the presence of B-9B in the depression, it is reasonable to assume that melt has increased following the Mertz calving, as indeed suggested by the observed freshening of the mixed layer in 2011 [*Shadwick et al.*, 2013]. Prior to the calving our estimates indicate that sea ice melt was a very small contribution to the freshwater budget of the area and, as for the ice production, did not show a strong relationship to the bottom salinity change in the depression. Yet, a substantial increase of the ice melt, reaching more than 10% of the decrease in the polynya ice production, occurred after the calving. The estimated surface melt rates do not take into account basal ice melt by the ocean, which may be very efficient in increasing the ice loss. Monitoring of ice melt may become increasingly important in order to estimate the evolution of the freshwater budget, and ultimately of the change in water mass properties in the region.

The estimated ice melt rates in the AD-tot region are not large enough to compensate the ice production, leading to an imbalance of the freshwater budget (Figure 4b). This is compatible with a latent heat polynya behavior where, on average, ice is exported out of the production area leading to net ice production. In CB mooring observations show that freshening occurs throughout the year and at all levels, including the deepest ones that are isolated from the Adélie Depression by a sill. The mechanisms underpinning this freshwater input such as vertical advection/diffusion with the overlying layer or sucking of the dense water over the sills need to be further investigated.

The freshwater source needed to close the freshwater budget in the Adélie Depression cannot be directly estimated from our too sparse observations. However, it can be estimated as a residual of the balance between the net ice production and the change in the mean salinity of the Adélie Depression. Assuming that the latter change is just equal to the bottom salinity change, an increase of at most 0.75 m a^{-1} (assuming a reference salinity of 34.50) of the freshwater content would be obtained in the depression over the 2010–2011 post calving period associated with a freshwater removal of 2.90 m a^{-1} by net ice production in the polynya (Figure 4b). A freshwater source of roughly 3.65 m a^{-1} would therefore be needed to balance the budget. The same calculation over the 2007–2009 precalving period indicates a slightly larger freshwater source of 3.85 m a^{-1} on average to equilibrate the net ice production (there is hardly any net salinity change over that period). Considering that these numbers are very rough estimates, we can therefore conclude there was only a slight decrease in the amount of "ambient" freshening between the precalving and postcalving period. This decrease, however, occurred despite enhanced melt of drift ice (by roughly 0.11 m an^{-1}) which we observed after

the calving. According to the MGT basal melt rate estimate of 11.4 Gt an^{-1} made by *Cougnon et al.* [2013] during the 1992–2007 period, glacier melting could only make a small contribution (on the order of at most 0.35 m an^{-1} if all the melt water was entering the depression) to the ambient freshening in the precalving period. The suppression of this contribution after the glacier tongue left the region in early April 2010 may, however, have contributed to the slight concomitant diminution of the ambient freshening.

5. Concluding Remarks

Repeated hydrographic observations collected over the summers 2004–2012 have allowed us to evaluate the interannual variability of the dense shelf waters in the MGP and to show that the recent deep freshening subsequent to the calving of part of the Mertz tongue was well beyond the range of this variability. A major consequence is that, within 2 years after the event, the bottom water of the shelf became too light to possibly contribute to renew the AABW in the AAB. This result also suggests that the shelf system does not have much inertia with regards to changes in the ice environment. A flushing time of the deep depression on the order of 1 year is indeed obtained if a dense outflow of 0.1 Sv [*Marsland et al.*, 2004; *Kusahara et al.*, 2011b; *Cougnon et al.*, 2013] is assumed.

Rough estimates of the freshwater budget of the Adélie Depression indicate that ambient freshening has not drastically changed after the Mertz calving, although being slightly reduced. This freshening includes several contributions like basal ice melt and ocean advection which individually may have been subject to abrupt changes after the glacier calving. A model study indeed suggests drastic changes of the shelf circulation in relation to the calving [*Kusahara et al.*, 2011b], which are likely to impact on the freshwater budget of the area.

The history of the year-to-year summer salinity changes over the period of observations mimics that of the preceding winter salinity. Prior to the calving, the convective system in the polynya was in a stratified state in which convection was partly controlled by the strength of the deep stratification. Exceptional events like the Mertz calving seem to be able to switch over the system to a new less stratified state where the system responds more directly to changes in the surface forcing. How long this new state is going to last will depend on the capacity of the polynya to restore deep reaching convection so that a new saline bottom layer can rebuild.

Appendix A: Correction Procedure Applied to the Seaguard Conductivity

In order to decide whether the time evolution of the conductivity recorded by the Seaguard in 2010 was reliable, we performed a comparison of the conductivities recorded by the same Seaguard in 2011 with the conductivities recorded by a Microcat moored on the same line only 2 dbar above. We found that in 2011 the offset between the two instruments varied in time and, upon detrending separately the two conductivity time series, different linear trends were indeed found (2.7×10^{-5} and 3.5×10^{-5} S m^{-1} d^{-1}, for the Seaguard and the Microcat, respectively). Moreover, the anomalies around the trends measured by the Seaguard revealed to be three times larger than those measured by the Microcat (0.0015 versus 0.0005 S m^{-1}), a result that was attributed to abnormal instrumental noise in the Seaguard. Yet the anomalies were reasonably correlated (0.708, $p = 0.01$) between the two instruments, implying that Seaguard anomalies, once normalized to their standard deviation (std), could be used, at least for the sake of a qualitative description of the bottom properties in 2010. Based on the 2011 data, we therefore built a model of "pseudoconductivities" taking the Seaguard measurements as input data and we applied it to the 2010 Seaguard data. The reconstructed pseudoconductivity time series for 2010 was obtained by calculating anomalies, C'_{est_10}, estimated from the 2010 Seaguard anomalies, C'_{S_10}, as $C'_{est\_10} = a\,C'_{S\_10} + b$ (where a and b were coefficients derived in 2011 from the linear regression of the Seaguard anomalies onto the bottom Microcat anomalies). The anomalies were then superimposed to a linear trend, $T_{CTD\_10} = 3.5 \times 10^{-5}$ S m^{-1} d^{-1}, deduced from two CTD casts carried out in the vicinity of the mooring in January 2010 and January 2011, respectively. Note that applying such a model to the bottom conductivity recorded by the Seaguard in 2011 results in a rms difference of 0.0048 between the estimated "pseudo" salinity and the Microcat "true" salinity.

References

Aoki, S., S. R. Rintoul, S. Ushio, S. Watanabe, and N. L. Bindoff (2005), Freshening of the Adélie Land Bottom Water near 140°E, *Geophys. Res. Lett.*, *32*, L23601, doi:10.1029/2005GL024246.

Beaman, R. J., P. E. O'Brien, A. L. Post, and L. De Santis (2011), A new high-resolution bathymetry model for the Terre Adélie and George V continental margin, East Antarctica, *Antarct. Sci.*, *23*, 95–103, doi:10.1017/S095410201000074X.

Bindoff, N. L., M. A. Rosenberg, and M. J. Warner (2000), On the circulation and water-masses over the Antarctic continental slope and rise between 80 and 150_E, *Deep Sea Res., Part II*, *47*, 2299–3326.

Bindoff, N. L., G. D. Williams, and I. Allison (2001), Sea-ice growth and water-mass modification in the Mertz Glacier polynya, East Antarctica, during winter, *Ann. Glaciol.*, *33*, 399–406.

Carmack, E. C. (1977), Water characteristics of the Southern Ocean south of the Polar Front, in *A Voyage of Discovery*, edited by M. V. Angel, pp. 15–41, Pergamon, Oxford, U. K.

Cavalieri, D. J., T. Markus, and J. C. Comiso (2004), AMSR-E/Aqua Daily L3 6.25 km 89 GHz Brightness Temperature Polar Grids. Version 2. Natl. Snow and Ice Data Cent., Boulder, Colo.

Cougnon, E. A., B. K. Galton-Fenzi, A. J. S. Meijers, and B. Legresy (2013), Modeling interannual dense shelf water export in the region of the Mertz Glacier Tongue (1992–2007), *J. Geophys. Res. Oceans*, *118*, 5858–5872, doi:10.1002/2013JC008790.

Dee, D. P., et al. (2011), The ERA-interim reanalysis: Configuration and performance of the data assimilation system, *Q. J. R. Meteorol. Soc.*, *137*, 553–597, doi:10.1002/qj.828.

Fraser, A. D., R. A. Massom, and K. J. Michael (2010), Generation of high-resolution East Antarctic landfast sea-ice maps from cloud-free MODIS satellite composite imagery, *Remote Sens. Environ.*, *114*, 2888–2896, doi:10.1016/j.rse.2010.07.006.

Fraser, A. D., R. A. Massom, K. J. Michael, B. K. Galton-Fenzi, and J. L. Lieser (2012), East Antarctic landfast sea ice distribution and variability, 2000-08, *J. Clim.*, *25*, 1137–1156, doi:10.1175/JCLI-D-10–05032.1.

Frezzotti, M., A. Cimbelli, and J. G. Ferrigno (1998), Ice-front change and iceberg behaviour along Oates and George V coasts, Antarctica, 1912–96, *Ann. Glaciol.*, *27*, 643–650.

Galton-Fenzi, B. K., J. R. Hunter, R. Coleman, S. J. Marsland, and R. C. Warner (2012), Modeling the basal melting and marine ice accretion of the Amery Ice Shelf, *J. Geophys. Res.*, *117*, C09031, doi:10.1029/2012JC008214.

Gordon, A. L., and P. Tchernia (1972), Waters of the continental margin off Adélie Coast, Antarctica, in *Antarctic Oceanology II: The Australian-New Zealand Sector, Antarct. Res. Ser.*, vol. 19, edited by D. E. Hayes, pp. 59–69, AGU, Washington, D. C.

Inoue, J., J. Ono, Y. Tachibana, M. Honda, K. Iwamoto, Y. Fujiyoshi, and K. Takeuchi (2003), Characteristics of heat transfer over the ice covered Sea of Okhotsk during cold-air outbreaks, *J. Meteorol. Soc. Jpn.*, *5*, 1057–1067.

Jacobs, S. S. (2004), Bottom water production and its links with the thermohaline circulation, *Antarct. Sci.*, *16*, 427–437.

Johnson, G. C., S. G. Purkey, and J. L. Bullister (2008), Warming and freshening in the abyssal southeastern Indian Ocean, *J. Clim.*, *21*, 5353–5365.

Kaleschke, L., X. Tian-Kunze, N. Maass, M. Mäkynen, and M. Drusch (2012), Sea ice thickness retrieval from SMOS brightness temperatures during the Arctic freeze-up period, *Geophys. Res. Lett.*, *39*, L05501, doi:10.1029/2012GL050916.

Koubbi, P., C. O'Brien, C. Loots, C. Giraldo, M. Smith, E. Tavernier, M. Vacchi, C. Vallet, J. Chevalier, and M. Moteki (2011), Spatial distribution and inter-annual variations in the size frequency distribution and abundances of Pleuragramma antarcticum larvae in the Dumont d'Urville Sea from 2004 to 2010, *Polar Sci.*, *5*, 225–238.

Kusahara, K., H. Hasumi, and G. D. Williams (2011a), Impact of the Mertz Glacier Tongue calving on dense water formation and export, *Nat. Commun.*, *2*, 159, doi:10.1038/ncomms1156.

Kusahara, K., H. Hasumi, and G. D. Williams (2011b), Dense shelf water formation and brine-driven circulation in the Adélie Depression, *Ocean Modell.*, *37*, 122–138, doi:10.1016/j.ocemod.20011.01.008.

Lacarra, M., M.-N. Houssais, E. Sultan, S. R. Rintoul, and C. Herbaut (2011), Summer hydrography on the shelf off Terre Adélie/George V Land based on the ALBION and CEAMARC observations during the IPY, *Polar Sci.*, *5*, 88–103, doi:10.1016/j.polar.2011.04.008.

Marsland, S. J., N. L. Bindoff, G. D. Williams, and W. F. Budd (2004), Modeling water mass formation in the Mertz Glacier Polynya and Adélie Depression, East Antarctica, *J. Geophys. Res.*, *109*, C11003, doi:10.1029/2004JC002441.

Marsland, S. J., J. A. Church, N. L. Bindoff, and G. D. Williams (2007), Antarctic coastal polynya response to climate change, *J. Geophys. Res.*, *112*, C07009, doi:10.1029/2005JC003291.

Martin, S., R. Drucker, R. Kwok, and B. Holt (2005), Improvements in the estimates of ice thickness and production in the Chukchi Sea polynyas derived from AMSR-E, *Geophys. Res. Lett.*, *32*, L05505, doi:10.1029/2004GL022013.

Massom, R. A., P. T. Harris, K. J. Michael, and M. J. Potter (1998), The distribution and formative processes of latent-heat polynyas in East Antarctica, *Ann. Glaciol.*, *27*, 420–426.

Masuda, S., et al. (2010), Simulated rapid warming of abyssal North Pacific water, *Science*, *329*, 319–322, doi:10.1126/science.1188703.

Naoki, K., J. Ukita, F. Nishio, M. Nakayama, J. C. Comiso, and A. Gasiewski (2008), Thin sea ice thickness as inferred from passive microwave and in situ observations, *J. Geophys. Res.*, *113*, C02S16, doi:10.1029/2007JC004270.

Ohshima, K. I., et al. (2013), Antarctic Bottom Water production by intense sea-ice formation in the Cape Darnley polynya, *Nat. Geosci.*, *6*, 235–240, doi:10.1038/NGEO1738.

Orsi, A. H. (2010), Recycling bottom waters, *Nat. Geosci.*, *3*, 307–309.

Orsi, A. H., G. C. Johnson, and J. L. Bullister (1999), Circulation, mixing, and production of Antarctic Bottom Water, *Prog. Oceanogr.*, *43*, 55–109.

Parkinson, C. L., and W. M. Washington (1979), A large-scale numerical model of sea ice, *J. Geophys. Res.*, *84*, 311–337.

Purkey, S. G., and G. C. Johnson (2012), Global contraction of Antarctic Bottom Water between 1980s and 2000s, *J. Clim.*, *25*, 5830–5844, doi:10.1175/JCLI-D-11–00612.1.

Rintoul, S. R. (1998), On the origin and influence of Adélie land bottom water, in *Ocean, Ice, and Atmosphere: Interactions at the Antarctic Continental Margin, Antarct. Res. Ser.*, vol. 75, edited by S. S. Jacobs and R. F. Weiss, pp. 151–171, AGU, Washington, D. C.

Rintoul, S. R. (2007), Rapid freshening of Antarctic Bottom Water formed in the Indian and Pacific oceans, *Geophys. Res. Lett.*, *34*, L06606, doi:10.029/2006GL028550.

Shadwick, E. H., S. R. Rintoul, B. Tillbrook, G. D. Williams, N. Young, A. D. Fraser, H. Marchant, J. Smith, and T. Tamura (2013), Glacier tongue calving reduced dense water formation and enhanced carbon uptake, *Geophys. Res. Lett.*, *40*, 904–909, doi:10.1002/grl.50178.

Shimada, K., S. Aoki, K. I. Ohshima, and S. Rintoul (2012), Influence of Ross Sea bottom water changes on the warming and freshening of the Antarctic bottom water in the Australian-Antarctic Basin, *Ocean Sci.*, *8*, 419–432, doi:10.5194/os-8–419-2012.

Spreen, G., L. Kaleschke, and G. Heygster (2008), Sea ice remote sensing using AMSR-E 89 GHz channels, *J. Geophys. Res.*, *113*, C02S03, doi:10.1029/2005JC003384.

Stouffer, R. J., D. Seidov, and B. J. Haupt (2007), Climate response to external sources of freshwater: North Atlantic versus the Southern Ocean, *J. Clim.*, *20*(3), 436–448, doi:10.1175/JCLI4015.1.

Tamura, T., K. I. Ohshima, T. Markus, D. J. Cavalieri, S. Nihashi, and N. Hirasawa (2007), Estimation of thin ice thickness and detection of fast ice from SSM/I data in the Antarctic Ocean, *J. Atmos. Oceanic Technol.*, *24*, 1757–1772.

Tamura, T., K. I. Ohshima, and S. Nihashi (2008), Mapping of sea ice production for Antarctic coastal polynyas, *Geophys. Res. Lett.*, *35*, L07606, doi:10.1029/2007GL032903.

Tamura, T., G. D. Williams, A. D. Fraser, and K. I. Ohshima (2012), Potential regimes shift in decreased sea ice production after the Mertz Glacier calving, *Nat. Commun.*, *3*, 826, doi:10.1038/ncomms1820.

Vaillancourt, R. D., R. N. Sambrotto, S. Green, and A. Matsuda (2003), Phytoplankton biomass and photosynthetic competency in the summertime Mertz Glacier region of East Antarctica, *Deep Sea Res., Part II*, *50*, 1415–1440.

Wendler, G., D. Gilmore, and J. Curtis (1997), On the formation of coastal polynyas in the area of Commonwealth Bay, Eastern Antarctica, *Atmos. Res.*, *45*, 55–75.

Whitworth, T., III (2002), Two modes of bottom water in the Australian-Antarctic Basin, *Geophys. Res. Lett.*, *29*(5), 1073, doi:10.1029/2001GL014282.

Whitworth, T., III, A. H. Orsi, S. J. Kim, W. D. Nowlin, and R. A. Locarnini (1998), Water masses and mixing near the Antarctic Slope Front, in *Ocean, Ice, and Atmosphere: Interactions at the Antarctic Continental Margin, Antarct. Res. Ser.*, vol. 75, edited by S. S. Jacobs and R. F. Weiss, pp. 1–27, AGU, Washington, D. C.

Williams, G. D., and N. L. Bindoff (2003), Wintertime oceanography of the Adélie Depression, *Deep Sea Res., Part II*, *50*, 1373–1392.

Zwally, H. J., M. B. Giovinetto, J. Li, H. G. Cornejo, M. A. Beckley, A. C. Brenner, J. L. Saba, and D. Yi (2005), Mass changes of the Greenland and Antarctic ice sheets and shelves and contributions to sea-level rise: 1992–2002, *J. Glaciol.*, *51*, 509–527.